Modeling and Nonlinear Backstepping Control of a 3-DoF Robot Manipulator

Abdelmajid Akil
Interdisciplinary Laboratory of Applied Sciences (LISA), ENSA Berrechid, Hassan 1 University, Settat, Morocco
abdelmajid.akil@gmail.com (corresponding author)

Ayoub Nouaiti
Department of Electrical Engineering, EST, Moulay Ismail University of Meknes, Morocco
nouayoub@gmail.com

Abdelwahed Touati
Laboratory of Complex Cyber Physical Systems (LCCPS), ENSAM, Hassan II University of Casablanca, Morocco
touati_2010@hotmail.com

Nabila Rabbah
Laboratory of Complex Cyber Physical Systems (LCCPS), ENSAM, Hassan II University of Casablanca, Morocco
nabila_rabbah@yahoo.fr

Received: 7 January 2025 | Revised: 23 February 2025 and 27 February 2025 | Accepted: 6 March 2025

 DOI: https://doi.org/10.48084/etasr.10145

ABSTRACT

Robotic manipulators face significant control challenges in a wide range of industrial applications, where stability and reliability are essential for achieving operational objectives. This paper investigates nonlinear modeling and control strategies for a three Degree-of-Freedom (3-DOF) robot manipulator, focusing on dynamic complexities and employing advanced techniques like nonlinear backstepping design for trajectory tracking. The 3-DOF robot's nonlinear model is derived using Lagrange's equation. Subsequently, a backstepping control method is developed to manage the nonlinear behavior. Backstepping ensures precise trajectory tracking and global stability by systematically designing a Lyapunov function for each step, leading to a robust control law. The step-by-step nature of backstepping facilitates the design of controllers for 3-DOF robotic systems. Each joint can be controlled separately while ensuring the overall stability of the system, making the design process more manageable. Simulation results demonstrate the ability of the proposed control method to achieve fast and accurate tracking of reference setpoints, even under moderate control input variations. These results highlight the effectiveness of the approach in enhancing both accuracy and stability.

Keywords-three Degree-of-Freedom robot manipulator; backstepping; nonlinear control; Lyapunov function

I. INTRODUCTION

Modeling and designing effective controllers for robot manipulators is a significant challenge due to their nonlinear dynamics and intricate mechanical structures. These systems are multi-input, multi-output, characterized by rapidly changing dynamics, numerous parameters, and uncertainties such as unknown loads and external disturbances. The development of accurate mathematical models and control strategies is complicated by factors such as design complexity, environmental conditions, and specific task requirements. To address these challenges, various techniques have been proposed in the literature for regulating the motion of robotic manipulators. In [1], a dynamic model is derived using Lagrange's equation, and a robust control approach combining sliding mode control with a PID control scheme is introduced. In [2], the trajectory tracking control for a nonlinear three-link robot manipulator is presented, where computed torque control and sliding mode control strategies are utilized. In [3], a cerebellar control model is proposed, which uses a feedback motor controller to train an artificial neural network. In [4], a control system incorporating fractional-order controllers is designed to eliminate vibrations leveraging singular

perturbation theory and input-state linearization techniques. In [5], fractional calculus theory is applied to design a finite-time fault-tolerant controller using a fractional-order adaptive backstepping approach, ensuring fast response and high-precision tracking performance. In addition, authors in [6] present a fractional-order system model for a robotic arm and the development of a fractional-order PID controller. In [7], a nonlinear backstepping controller with a velocity observer is proposed for trajectory tracking control. Meanwhile, authors in [8] suggest combining a neural network with adaptive sliding mode control for trajectory tracking of a three Degree-of-Freedom (3-DOF) planar parallel manipulator. Sliding-mode control strategies for trajectory tracking are also discussed in [9] and [8]. Lastly, authors in [10] present a software-in-the-loop test for a robot manipulator driven by a brushless DC motor. Two different control approaches, such as the classical PID control and the fractional-order PID control are used in [11] to improve the tracking performance of the manipulator under study. Classic control methods like PID, which do not account for system nonlinearity, and sliding mode control methods, which involve complex calculations, can result in significant computational differences that can weaken the overall control performance. However, backstepping is specifically designed for nonlinear systems, making it suitable for complex and highly nonlinear control problems. Several works have demonstrated the effectiveness of the backstepping control method for different applications such as in [12, 13]. A key advantage of this approach is its flexibility in formulating the control law without requiring the cancellation of beneficial nonlinearities. The main contributions of this study include the development of a mathematical model for a 3-DOF robot manipulator and the design of a backstepping nonlinear control strategy for it. This control law is systematic, robust, and asymptotically stable based on Lyapunov stability theory.

II. DESCRIPTION OF 3-DOF ROBOT MANIPULATOR

The mobile manipulator under study is shown in Figure 1. It consists of two subsystems: a rotating base and two planar rotating joints (link 1 and link 2).

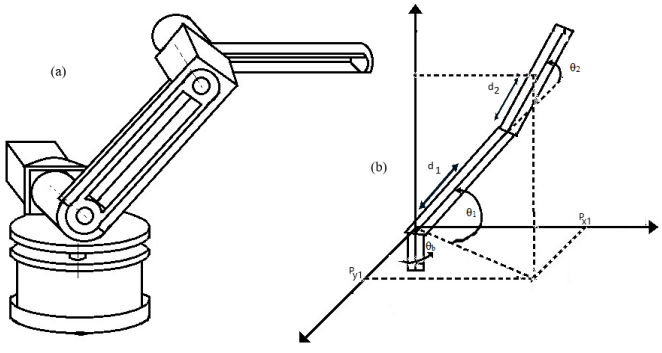

Fig. 1. (a) 3-DOF physical system (b) spherical coordinates.

The base, equipped with an actuator, rotates around a vertical axis by an angle θ_b. The second subsystem includes two masses, m_1 and m_2, connected by weightless bars of half lengths d_1 and d_2. Each joint is driven by a DC servo motor to enable arm movement. The angles θ_1 and θ_2 represent the rotations of the first bar around the origin and the second bar around the endpoint of the first bar, respectively. Consequently, the system has three degrees of freedom: θ_b, θ_1, and θ_2.

III. MATHEMATICAL MODEL OF 3-DOF ROBOT MANIPULATOR

A. Kinematic Relationships

The equations for the x-position and y-position of link 1 are:

$$\begin{cases} p_{x_1} = d_1 \cos(\theta_1) \\ p_{y_1} = d_1 \sin(\theta_1) \end{cases} \quad (1)$$

The equations for the x-position and y-position of link 2 are:

$$\begin{cases} P_{x_2} = 2d_1 \cos(\theta_1) + d_2 \cos(\theta_1 + \theta_2) \\ P_{y_2} = 2d_1 \sin(\theta_1) + d_2 \sin(\theta_1 + \theta_2) \end{cases} \quad (2)$$

The linear velocities of link 1 and link 2 are calculated using the following formulas:

$$v_1 = \sqrt{\dot{p}_{x_1}^2 + \dot{p}_{y_1}^2}, \text{ where: } \begin{cases} \dot{p}_{x_1}^2 = d_1^2 \dot{\theta}_1^2 \sin^2(\theta_1) \\ \dot{p}_{y_1}^2 = d_1^2 \dot{\theta}_1^2 \cos^2(\theta_1) \end{cases} \quad (3)$$

and $v_2 = \sqrt{\dot{p}_{x_2}^2 + \dot{p}_{y_2}^2}$, where:

$$\begin{cases} \dot{p}_{x_2}^2 = 4\, d_1^2 \dot{\theta}_1^2 \sin^2(\theta_1) + 4 d_1 d_2 \dot{\theta}_1 (\dot{\theta}_1 + \dot{\theta}_2) \sin(\theta_1) \\ \quad \sin(\theta_1 + \theta_2) + d_2^2 (\dot{\theta}_1 + \dot{\theta}_2)^2 \sin^2(\theta_1 + \theta_2) \\ \dot{p}_{y_2}^2 = 4\, 4\, d_1^2 \dot{\theta}_1^2 \cos^2(\theta_1) + 4 d_1 d_2 \dot{\theta}_1 (\dot{\theta}_1 + \dot{\theta}_2) \cos(\theta_1) \\ \quad \cos(\theta_1 + \theta_2) + d_2^2 (\dot{\theta}_1 + \dot{\theta}_2)^2 \cos^2(\theta_1 + \theta_2) \end{cases} \quad (4)$$

with the derivative with respect to time t, i.e., $\dot{\theta}_i = \frac{d\theta_i}{dt}$, $\dot{y}_i = \frac{dy_i}{dt}$, $\dot{x}_i = \frac{dx_i}{dt}$, for $i = 1; 2$. The angular velocities of link 1 and link 2 are calculated using the formulas $\omega_i = \dot{\theta}_i$ and $\omega_i = \dot{\varphi}$.

B. Energetic Relationships

The equation of the kinetic energy for link $i = 1; 2$ is:

$$K_i = \frac{1}{2} m_i v_i^2 \quad (5)$$

The equation for the kinetic energy K can be written as:

$$K = K_1 + K_2 = \frac{1}{2} m_1 d_1^2 \dot{\theta}_1^2 + m_2 \{2\, d_1^2 \dot{\theta}_1^2 + \frac{1}{2} d_2^2 (\dot{\theta}_1 + \dot{\theta}_2)^2 + 2 d_1 d_2 \dot{\theta}_1 (\dot{\theta}_1 + \dot{\theta}_2) \cos(\theta_2)\} \quad (6)$$

The total potential energy P due to gravity is given by:

$$P = P_1 + P_2 = m_1 g d_1 \cos(\theta_1) + m_2 g (d_1 \cos(\theta_1) + d_2 \cos(\varphi)) \quad (7)$$

C. Dynamic Analysis

The classical nonlinear dynamic model of the 3-DOF robot manipulator is derived using Lagrange's equation, along with the equations for kinetic and potential energies. Its equation is defined as:

$$\frac{\partial}{\partial t} \frac{\partial \mathcal{L}}{\partial \dot{\theta}_i} - \frac{\partial \mathcal{L}}{\partial \theta_i} = \tau_i \quad (8)$$

where θ_i, $\dot{\theta}_i$ represent the joint position and joint velocity, and τ_i is the generalized force applied to the i-th link.

The equations of motion, derived using the Euler-Lagrange equation, are obtained by taking the difference between the total kinetic energy K and the total potential energy P of a mechanical system to determine the Lagrangian $\mathcal{L}$ of the system. This allows us to calculate the forces or torques applied at each link. The Lagrangian is defined as follows:

$$\mathcal{L} = K - P = \frac{1}{2}m_1 d_1^2\dot{\theta}_1^2 + m_2\{2\, d_1^2\dot{\theta}_1^2 + \frac{1}{2}d_2^2\,(\dot{\theta}_1 + \dot{\theta}_2)^2 + 2d_1 d_2(\dot{\theta}_1^2 + \dot{\theta}_1\dot{\theta}_2)\cos(\theta_2)\} - m_1 g d_1\cos(\theta_1) - m_2 g(d_1\cos(\theta_1) + d_2\cos(\theta_1+\theta_2)) \quad (9)$$

The derivations of the Lagrangian and the Euler-Lagrange equations are given as follows:

$$\frac{\partial\mathcal{L}}{\partial\dot{\theta}_1} = m_1 d_1^2\dot{\theta}_1 + m_2\big(4\, d_1^2\dot{\theta}_1 + d_2^2\,(\dot{\theta}_1+\dot{\theta}_2) + 2d_1 d_2(2\dot{\theta}_1 + \dot{\theta}_2)\cos(\theta_2)\big) \quad (10)$$

$$\frac{\partial}{\partial t}\frac{\partial\mathcal{L}}{\partial\dot{\theta}_1} = m_1 d_1^2\ddot{\theta}_1 + m_2\{4d_1^2\ddot{\theta}_1 + d_2^2\,(\ddot{\theta}_1+\ddot{\theta}_2) + 2d_1 d_2\big(2\ddot{\theta}_1\cos(\theta_2) - 2\dot{\theta}_1\,\dot{\theta}_2\sin(\theta_2) + \ddot{\theta}_2\cos(\theta_2) - \dot{\theta}_2^2\sin(\theta_2)\big)\} \quad (11)$$

$$\frac{\partial\mathcal{L}}{\partial\theta_1} = m_1 g d_1\sin(\theta_1) + m_2 g(d_1\sin(\theta_1) + d_2\sin(\theta_1+\theta_2)) \quad (12)$$

Similarly, we compute:

$$\frac{\partial\mathcal{L}}{\partial\dot{\theta}_2} = m_2\big(\, d_2^2\,(\dot{\theta}_1+\dot{\theta}_2) + 2d_1 d_2\dot{\theta}_1\cos(\theta_2)\big) \quad (13)$$

$$\frac{\partial}{\partial t}\frac{\partial\mathcal{L}}{\partial\dot{\theta}_2} = m_2\big(\, d_2^2\,(\ddot{\theta}_1+\ddot{\theta}_2) + 2d_1 d_2\ddot{\theta}_1\cos(\theta_2) - 2d_1 d_2\dot{\theta}_1\dot{\theta}_2\sin(\theta_2)\big) \quad (14)$$

$$\frac{\partial L}{\partial\theta_2} = -2m_2 d_1 d_2\big(\dot{\theta}_1^2 + \dot{\theta}_1\dot{\theta}_2\,\big)\sin(\theta_2) + m_2 g(d_2\sin(\theta_1+\theta_2)) \quad (15)$$

D. DC Servo Motor Model

The mathematical model of a DC servo motor describes the dynamic relationship between the input (voltage) and the output (position). The internal structure of the DC servo motor is shown in Figure 2. Here, J represents the moment of inertia of the load attached to the motor's drive shaft.

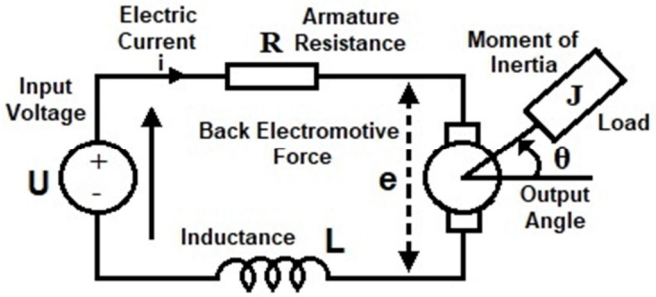

Fig. 2. Electro-mechanical scheme of a DC motor.

The electrical differential equation for a DC servo motor can be expressed as follows:

$$u_j(t) = K_e N_j\dot{\theta}_j(t) + R\; i_j(t) + L\frac{di_j}{dt} + \varepsilon_j \quad (16)$$

Let $i_j(t)$ be the armature current and $u_j(t)$ be the voltage applied to the armature. R, L and ε_j represent the resistance, inductance, and the back Electromotive Force (EMF) of the armature, respectively; $\dot{\theta}_j$ is the angular velocity, and N_j is the gear ratio, where $j = 1; 2; b$. The first-order differential equation for $i_j(t)$ is:

$$\frac{di_j}{dt} = \frac{-1}{L}\big[N_j K_e\dot{\theta}_1 + R\; i_j + \varepsilon - u_j\big] \quad (17)$$

The equation of motion for the rotor is derived using Newton's second law of rotation. The DC servo motor torque can also be written as:

$$T = N_j K_T i = J_e\dot{\omega} + B_e\omega + T_f \quad (18)$$

where K_T (Nm/A) is the torque constant.

The friction torque T_f opposes the motor torque, where J_e and B_e are the moment of inertia and the friction coefficient of the motor and load, respectively. By substituting (22) into (23), we obtain the following expression for the armature current:

$$i_j(t) = \frac{J_e}{N_j K_T}\dot{\omega}_j + \frac{B_e}{N_j K_T}\omega_j + \frac{1}{N_j K_T}T_f \quad (19)$$

E. Global Model

The nonlinear mathematical model used to construct the robust control based on backstepping is derived as follows. The state variables of the system are defined as: $x_1 = \theta_b$, $x_2 = \dot{\theta}_b$, $x_3 = i_b$, $x_4 = \theta_1$, $x_5 = \dot{\theta}_1$, $x_6 = i_1$, $x_7 = \theta_2$, $x_8 = \dot{\theta}_2$, $x_9 = i_2$. The state vector of the system is $x = [\theta_b, \theta_1, \theta_2]^{\,t}$, and the control input vector is denoted as $u = [u_b, u_1, u_2]^{\,t}$. The complete model of the 3-DOF robot manipulator is given by the following equations for the subsystems Sys 1, Sys 2, and Sys 3. The equation for the subsystem Sys 1 is:

$$\dot{x}_1 = x_2 \quad (20)$$

$$\dot{x}_2 = \frac{-K_T}{N_b J_e}\Big[\frac{B_e}{K_T}N_b x_2 + \frac{1}{K_T}T_f - x_3\Big] \quad (21)$$

$$\dot{x}_3 = \frac{-1}{L}[K_e N_b x_2 + R\; x_3 - u_b + \varepsilon_b] \quad (22)$$

The equation for the subsystem Sys 2 is:

$$\dot{x}_4 = x_5 \quad (23)$$

$$\dot{x}_5 = \frac{-1}{(m_1 d_1^2 + m_2 4d_1^2 + m_2 d_2^2 + 4m_2 d_1 d_2\cos(x_7))}\{m_2\big(\, d_2^2\dot{x}_8 + 2d_1 d_2(-2x_5\, x_8\sin(x_7) + \dot{x}_8\cos(x_7) - x_7^2\sin(x_7))\big) - m_1 g d_1\sin(x_4) - m_2 g(d_1\sin(x_4) + d_2\sin(x_4+x_7)) - N_1 K_T x_6\} \quad (24)$$

$$\dot{x}_6 = \frac{-1}{L}[N_1 K_e x_5 + R\; x_6 + \varepsilon_1 - u_1] \quad (25)$$

The equation for the subsystem Sys 3 is:

$$\dot{x}_7 = x_8 \quad (26)$$

$$\dot{x}_8 = \frac{-1}{4l_2^2 m_2}\{(4d_2^2 m_2 + 2m_2 d_1 d_2 \cos(x_7))\dot{x}_5 -$$

$$2m_2 d_1 d_2 x_5 x_8 \sin(x_7) + 2m_2 d_1 d_2 (x_5^2 + x_5 x_8)\sin(x_7) + m_2 g(d_2 \sin(x_4 + x_7)) - N_2 K_T x_9\} \quad (27)$$

$$\dot{x}_9 = \frac{-1}{L}[N_2 K_e x_8 + R\, x_9 + \varepsilon_2 - u_2] \quad (28)$$

The first subsystem has the state vector θ_b, controlled by the voltage u_b, the second subsystem has the state vector θ_1, controlled by u_1, and the third subsystem has the state vector θ_2, controlled by u_2. A general mathematical model of a 3-DOF robot manipulator with rigid links and a rotary base is multivariable, strongly coupled, nonlinear, and time-varying. This model is typically sufficient for control synthesis.

IV. NONLINEAR BACKSTEPPING DESIGN OF 3-DOF ROBOT MANIPULATOR

The backstepping controller system is designed to stabilize the robot's motion by addressing the dynamics of each subsystem and ensuring robust performance under different operating conditions. For each system (h) with $h = 1; 2; 3$, the number of design steps required is equal to 3. In each step, an error variable ζ_{li} and a stabilizing function α_{lj} with $i = 1; 2; 3$, $j = 0,1,2$, and $l = b; 1; 2$ are designed.

A. Backstepping Controller for Rotating Base

Step 1: The tracking error between the motor position at the base and desired position $x_1^r = \theta_b^r$ is defined as:

$$\zeta_{b1} = x_1 - x_1^r \quad (29)$$

$$\Longrightarrow \dot{\zeta}_{b1} = \dot{x}_1 - \dot{x}_1^r = x_2 - \dot{x}_1^r \quad (30)$$

Using (30), the virtual controller is:

$$\alpha_{b0} = x_2 = -c_1 \zeta_{b1} + \dot{x}_1^r \quad (31)$$

by using α_{b0} as the virtual control input. The previous equation can be expressed as:

$$\dot{\zeta}_{b1} = -c_1 \zeta_{b1} \quad (32)$$

where the controller gain parameter c_1 is a positive constant.

Step 2: The error between x_2 and α_{b0} tends towards 0 as possible:

$$\zeta_{b2} = x_2 - \alpha_{b0} \quad (33)$$

$$\Rightarrow \dot{\zeta}_{b2} = \frac{-1}{L}[K_e N_b x_2 + R\, x_3 - u_b + \varepsilon_b] - \dot{\alpha}_{b0} \quad (34)$$

The virtual controller is chosen as:

$$\alpha_{b1} = x_3 = \frac{1}{R}[K_e N_b x_2 - u_b + \varepsilon_b + L\dot{\alpha}_0 - Lc_2\varsigma_1] \quad (35)$$

by using α_1 as the virtual control input. The previous equation can be expressed as:

$$\dot{\zeta}_{b2} = -c_2 \zeta_{b2} \quad (37)$$

where controller gain parameter c_2 is a positive constant.

Step 3 (final): The error between x_3 and α_{b1} is driven towards 0 as possible:

$$\zeta_{b3} = x_3 - \alpha_{b1} \quad (37)$$

$$\Longrightarrow \dot{\zeta}_{b3} = \frac{-1}{L}[K_e N_b x_2 + R\, x_3 + \varepsilon_b + L\dot{\alpha}_{b1}] + \frac{1}{L}u_b \quad (38)$$

The effective command input u_b can be expressed as:

$$u_b(t) = -c_3 \zeta_b + \frac{1}{L}[K_e N_b x_2 + R\, x_3 + \varepsilon_b + L\dot{\alpha}_{b1}] \quad (39)$$

For this, the previous equation can be expressed as:

$$\dot{\zeta}_{b3} = -c_3 \zeta_{b3} \quad (40)$$

where the controller gain parameter c_3 is a positive constant. The derivative of the candidate Lyapunov function is given by:

$$\dot{v}_1(t) = \zeta_{b1}\dot{\zeta}_{b1} + \zeta_{b2}\dot{\zeta}_{b2} + \zeta_{b3}\dot{\zeta}_{b3} \quad (41)$$

$$\Rightarrow \dot{v}_1(t) = -c_1\zeta_{b1}^2 - c_2\zeta_{b2}^2 - c_3\zeta_{b3}^2 < 0 \quad (42)$$

B. Backstepping Controllers for Link 1 and Link 2

The virtual controllers and effective commands for each link are determined using the same calculation steps described in this section. Only the results of each step are presented for link 1 and link 2.

1) Backstepping Controller for Link 1

Step1: The tracking error between the motor position x_1 and the desired position $x_1^r = \theta_1^r$ is defined as:

$$\varsigma_{11} = x_4 - x_4^r \quad (43)$$

The virtual controller is:

$$\alpha_{10} = x_5 = -c_4\varsigma_{11} + \dot{x}_4^r \quad (44)$$

The dynamics of the error is given by:

$$\dot{\varsigma}_{11} = -c_4\varsigma_{11} \quad (45)$$

where the controller gain parameter c_4 is a positive constant.

Step 2: The error between x_2 and the desired position α_{10} tends towards 0 as possible:

$$\varsigma_{12} = x_5 - \alpha_{10} \quad (46)$$

The virtual controller is:

$$\alpha_{11} = -\frac{(m_1 d_1^2 + m_2 4d_1^2 + m_2 d_2^2 + 4m_2 d_1 d_2 \cos(x_7))}{N_1 K_T}(c_5\varsigma_1 - \dot{\alpha}_{10}) + \{m_2\Big(d_2^2\dot{x}_8 + 2d_1 d_2(-2x_5 x_8 \sin(x_7) + \dot{x}_8 \cos(x_7) - x_7^2 \sin(x_7))\Big) - m_1 g d_1 \sin(x_4) - m_2 g(d_1 \sin(x_4) + d_2 \sin(x_4 + x_7))\} \quad (47)$$

The dynamics of the error is given by:

$$\dot{\varsigma}_{12} = -c_5\varsigma_{12} \quad (48)$$

where the controller gain parameter c_5 is a positive constant.

Step 3: The error between x_3 and α_{11} tends towards 0 as possible:

$$\varsigma_{13} = x_6 - \alpha_{11} \quad (49)$$

The effective command input u_1 can be expressed as:

$$u_1(t) = -Lc_2\varrho_{13} + N_1K_e x_5 + R\, x_6 + \varepsilon_1 + L\dot{\alpha}_{11} \quad (50)$$

The dynamics of the error is given by:

$$\dot{\varsigma}_{13} = -c_6\varsigma_{13} \quad (51)$$

where the controller gain parameter c_6 is a positive constant. The derivative of the candidate Lyapunov function is given by:

$$\dot{v}_1(t) = \varsigma_{11}\dot{\varsigma}_{11} + \varsigma_{12}\dot{\varsigma}_{12} + \varsigma_{13}\dot{\varsigma}_{13} \quad (52)$$

$$\Rightarrow \dot{v}_1(t) = -c_4\varsigma_{11}^2 - c_5\varsigma_{12}^2 - c_6\varsigma_{13}^2 < 0 \quad (53)$$

2) Backstepping Controller for Link 2

Step1: The tracking error between the motor position x_7 and the desired position $x_7^r = \theta_2^r$ is defined as:

$$\varrho_{21} = x_7 - x_7^r \quad (54)$$

The virtual controller is:

$$\alpha_{21} = x_8 = -c_7\varrho_{21} + \dot{x}_7^r \quad (55)$$

The dynamics of the error is given by:

$$\dot{\varrho}_{21} = -c_7\varrho_{21} \quad (56)$$

where the controller gain parameter c_7 is a positive constant.

Step 2: The error between x_8 and the desired position α_{21} tends towards 0 as possible:

$$\varrho_{22} = x_8 - \alpha_{21} \quad (57)$$

The virtual controller is:

$$\alpha_{22} = x_9 = -\frac{4l_2^2m_2}{N_2K_T}(c_8\varrho_{22} - \dot{\alpha}_{21}) + \frac{1}{N_2K_T}\{(4d_2^2m_2 + 2m_2d_1d_2\cos(x_7))\dot{x}_5 - 2m_2d_1d_2x_5x_8\sin(x_7) + 2m_2d_1d_2(x_5^2 + x_5x_8).\sin(x_7) + m_2g(d_2\sin(x_4 + x_7))\} \quad (58)$$

The dynamics of the error is given by:

$$\dot{\varrho}_{22} = -c_8\varrho_{22} \quad (59)$$

where the controller gain parameter c_8 is a positive constant.

Step 3: The error between x_9 and α_{22} tends towards 0 as possible:

$$\varrho_{23} = x_9 - \alpha_{22} \quad (60)$$

The effective command input u_2 can be expressed as:

$$u_2(t) = -L(c_9\varrho_{23} - \dot{\alpha}_{22}) - [N_2K_e x_8 + R\, x_9 + \varepsilon_2] \quad (61)$$

The dynamics of the error is given by:

$$\dot{\varrho}_{23} = -c_9\varrho_{23} \quad (62)$$

where the controller gain parameter c_9 is a positive constant. The derivative of the candidate Lyapunov function is given by:

$$\dot{v}_2(t) = \varrho_{21}\dot{\varrho}_{21} + \varrho_{22}\dot{\varrho}_{22} + \varrho_{23}\dot{\varrho}_{23} \quad (63)$$

$$\dot{v}_2(t) = -c_7\varrho_{21}^2 - c_8\varrho_{22}^2 - c_9\varrho_{23}^2 < 0 \quad (64)$$

C. Global Backstepping Controller

Considering the backstepping control input vector:

$$u_b(t) = -c_3\zeta_b + \frac{1}{L}[K_eN_bx_2 + R\, x_3 + \varepsilon_b + L\dot{\alpha}_{b2}] \quad (65)$$

$$u_1(t) = -Lc_2\varrho_{13} + N_1K_e x_5 + R\, x_6 + \varepsilon_1 + L\dot{\alpha}_{12} \quad (66)$$

$$u_2(t) = -L(c_9\varrho_{23} - \dot{\alpha}_{22}) - [N_2K_e x_8 + R\, x_9 + \varepsilon_2] \quad (67)$$

The backstepping controller is designed to stabilize the system using the following candidate Lyapunov function:

$$v(t) = v_b(t) + v_1(t) + v_2(t) \quad (68)$$

The derivative of v is given by:

$$\dot{v}(t) = \dot{v}_b(t) + \dot{v}_1(t) + \dot{v}_2(t) < 0 \quad (69)$$

The closed-loop system of the 3-DOF robot manipulator is globally asymptotically stable, which is achieved by the controllers designed for stabilization and tracking. A positive definite Lyapunov candidate function is used for stability analysis, and its negative definite derivative guarantees stability.

V. SIMULATION TESTS

To illustrate the effectiveness and performance of the proposed nonlinear backstepping control for the 3-DOF robot manipulator, simulation tests are conducted in Simulink, as shown in Figure 3. To analyze the performance of the tracking by backstepping controller, the base and joint angle transitions of the manipulator from the starting point to the target point along the desired trajectory are shown in Figures 4, 5, and 6. The results show that joint 1 has a response time of approximately 0.008 s, whereas joint 2 and the rotating base have a response time of about 4.8×10^{-3} s. The backstepping controller effectively tracks the desired trajectory for angles θ_1, θ_2, and θ_b, with minimal and acceptable angle errors that do not affect system performance. The system remains stable, with no divergence or chaotic behavior, and switches quickly between desired values. The continuous angular displacement curves confirm smooth robot movement, and the system achieves accurate position tracking without overshoot, undershoot, or oscillations.

VI. CONCLUSION

This study presents a comprehensive approach to modeling and controlling a three Degree-of-Freedom (3-DOF) robot manipulator. The developed mathematical model effectively captures the manipulator's dynamic and kinematic properties while addressing key challenges such as nonlinearity, coupling effects, and external disturbances. A backstepping controller is designed for each joint, and its stability is verified through Lyapunov analysis. This new control strategy is proposed to ensure the asymptotic stability of the whole system, as well as to improve the accuracy and the transient dynamic response of the 3-DOF robot. The accuracy and stability problem that many existing manipulators suffer from has been addressed using this classical control technique such as PID control. The effectiveness of the proposed control method is demonstrated through Simulink simulations, which confirm the feasibility, performance, and efficiency of the system. Future work will focus on experimental testing of the proposed manipulator system to further validate the approach.

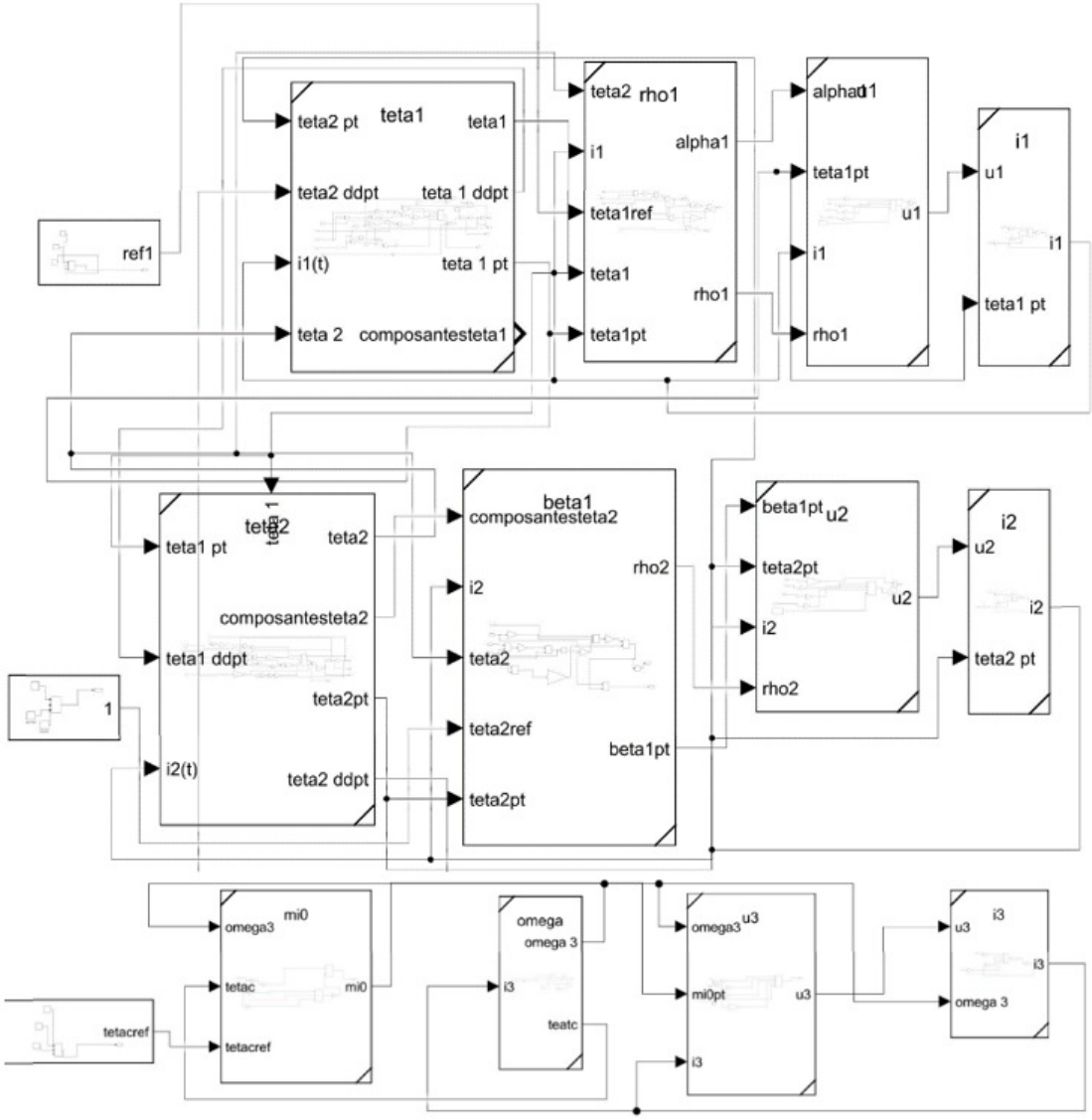

Fig. 3. The Simulink model and submodels for the backstepping controller.

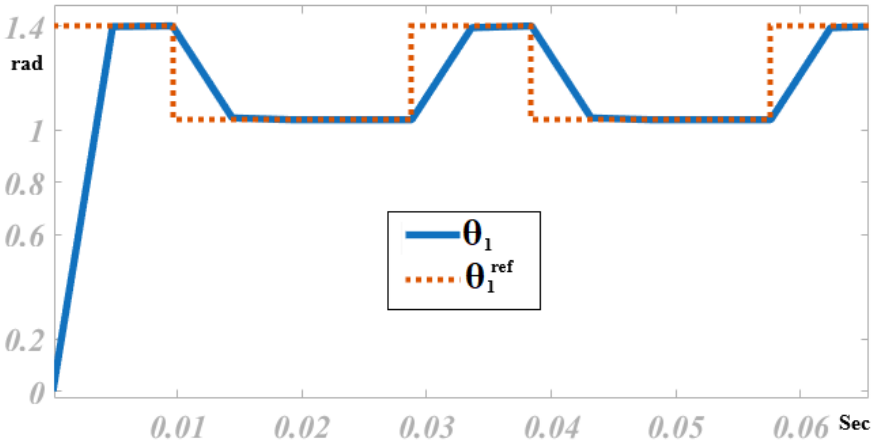

Fig. 4. Position tracking of the joint 1 with backstepping controller.

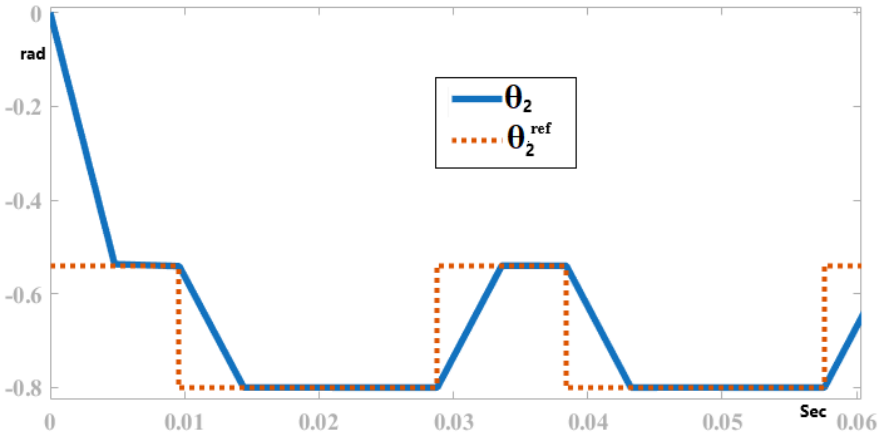

Fig. 5. Position tracking of the joint 2 with backstepping controller.

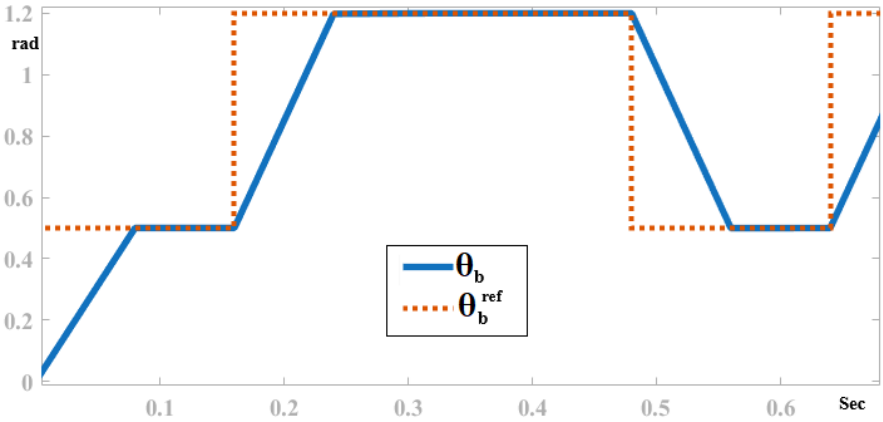

Fig. 6. Position tracking of the base with backstepping controller.

REFERENCES

[1] A. A. Mohammed and A. Eltayeb, "Dynamics and Control of a Two-link Manipulator using PID and Sliding Mode Control," in *2018 International Conference on Computer, Control, Electrical, and Electronics Engineering*, Khartoum, Sudan, 2018, pp. 1–5, https://doi.org/10.1109/ICCCEEE.2018.8515795.

[2] N. K. Chaturvedi and L. B. Prasad, "A Comparison of Computed Torque Control and Sliding Mode Control for a Three Link Robot Manipulator," in *2018 International Conference on Computing, Power and Communication Technologies*, Greater Noida, India, 2018, pp. 1019–1024, https://doi.org/10.1109/GUCON.2018.8675048.

[3] J. A. Romero, L. A. Diago, J. Shinoda, and I. Hagiwara, "Evaluation of Brain Models to Control a Robotic Origami Arm Using Holographic Neural Networks," in *39th Mechanisms and Robotics Conference*, Boston, MA, USA, 2015, https://doi.org/10.1115/DETC2015-48074.

[4] D. Feliu-Talegon and V. Feliu-Batlle, "Control of Very Lightweight 2-DOF Single-Link Flexible Robots Robust to Strain Gauge Sensor Disturbances: A Fractional-Order Approach," *IEEE Transactions on Control Systems Technology*, vol. 30, no. 1, pp. 14–29, Jan. 2022, https://doi.org/10.1109/TCST.2021.3053857.

[5] Z. Anjum and Y. Guo, "Finite Time Fractional-order Adaptive Backstepping Fault Tolerant Control of Robotic Manipulator," *International Journal of Control, Automation and Systems*, vol. 19, no. 1, pp. 301–310, Jan. 2021, https://doi.org/10.1007/s12555-019-0648-6.

[6] S. Husnain and R. Abdulkader, "Fractional Order Modeling and Control of an Articulated Robotic Arm," *Engineering, Technology & Applied Science Research*, vol. 13, no. 6, pp. 12026–12032, Dec. 2023, https://doi.org/10.48084/etasr.6270.

[7] F.-S. Chen and J.-S. Lin, "Nonlinear backstepping design of robot manipulators with velocity estimation feedback," in *2004 5th Asian Control Conference (IEEE Cat. No.04EX904)*, Melbourne, Australia, 2004, pp. 351–356 vol.1.

[8] T. N. Truong, H.-J. Kang, and T. D. Le, "Adaptive Neural Sliding Mode Control for 3-DOF Planar Parallel Manipulators," in *Proceedings of the 2019 3rd International Symposium on Computer Science and Intelligent Control*, Amsterdam, Netherlands, 2020, pp. 1–6, https://doi.org/10.1145/3386164.3387261.

[9] M. Zhou, Y. Feng, C. Xue, and F. Han, "Deep convolutional neural network based fractional-order terminal sliding-mode control for robotic manipulators," *Neurocomputing*, vol. 416, pp. 143–151, Nov. 2020, https://doi.org/10.1016/j.neucom.2019.04.087.

[10] M. B. Ayed, L. Zouari, and M. Abid, "Software In the Loop Simulation for Robot Manipulators," *Engineering, Technology & Applied Science Research*, vol. 7, no. 5, pp. 2017–2021, Oct. 2017, https://doi.org/10.48084/etasr.1285.

[11] A. Dumlu and K. Erenturk, "Trajectory Tracking Control for a 3-DOF Parallel Manipulator Using Fractional-Order $PI^{\lambda}D^{\mu}$ Control," *IEEE Transactions on Industrial Electronics*, vol. 61, no. 7, pp. 3417–3426, Jul. 2014, https://doi.org/10.1109/TIE.2013.2278964.

[12] Y. Li, S. Qiang, X. Zhuang, and O. Kaynak, "Robust and adaptive backstepping control for nonlinear systems using RBF neural networks," *IEEE Transactions on Neural Networks*, vol. 15, no. 3, pp. 693–701, May 2004, https://doi.org/10.1109/TNN.2004.826215.

[13] A. Akil, M. Zegrari, A. Touati, and N. Rabbah, "Nonlinear control by backstepping applied to the web winding system," *International Journal of Dynamics and Control*, vol. 8, no. 2, pp. 656–665, Jun. 2020, https://doi.org/10.1007/s40435-019-00568-z.